Fatigue crack propagation due to thermal shock in AISI 316 stainless steel

S. T. HASAN, M. W. BROWN
Department of Mechanical and Process Engineering,
University of Sheffield,
Mappin Street,
SHEFFIELD S1 3JD
U.K.

Third International Conference on Biaxial/Multiaxial Fatigue, April 3 - 6, 1989, Stuttgart, FRG.

ABSTRACT

An experimental study of fatigue crack propagation has been completed under thermal downshock conditions in 2 mm thick single edge and double edge cracked plates of type 316 stainless steel, cooled rapidly by an airjet from an initial temperature of 625°C. The effect of a superimposed static tensile stress on crack growth has been examined.

Growth is fast where small cracks are propagating in the high temperature gradient near cooled edges, but longer cracks slow down and arrest as they move into a region of compressive stress. A superimposed static tensile stress increases both the speed and penetration of cracks.

A strain analysis of the thermal stress field is presented, derived from measured temperature distributions. Predictions of fatigue crack growth behaviour due to thermal loading are made from isothermal data, and correlated with the experimental observations.

1. INTRODUCTION

Several studies of thermal downshock have been carried out in the past [1, 2, 3, 4]. Thermal fatigue is an important problem, which is relevant to power generating, aircraft, nuclear and process industries, extensive work has been carried out recently on austenitic and ferritic steels [5]. Early work was designed to compare the properties of different materials and to find those most resistant to crack growth

and nucleation [6]. However it is also important to understand the behaviour of propagating fatigue cracks during thermal shock, and their subsequent arrest. Fatigue fracture, or breakthrough of a crack has to be avoided in engineering applications, so the ability of cracks to arrest is a relevant aspect of safe high temperature design.

A simple approach has been presented for analysis of fatigue crack propagation and arrest behaviour by Misumi et al [7], but no life predictions have been made. Breakthrough of cracks was observed by Shimizu [8] for high temperatures in stainless steel, where creep mechanisms took precedence over fatigue. Skelton [9] and Marsh [10] have both reported that under thermal downshock conditions, life predictions can be made by correlating with isothermal data, at a representative temperature for the cycle.

In this paper a thermal stress analysis based on the strain intensity approach is presented, which reveals an oxide induced closure effect in pure thermal shock conditions at low growth rates. Experimental observations of both isothermal and single edge thermal shock results are correlated and predictions of growth rate can be made. Results may also be compared on the basis of stress intensity factor range, but it is observed that the strain intensity factor approach is more satisfactory for thermal stress conditions including both cyclic plasticity and a range of temperature.

Further work is required to define a better elastic-plastic parameter, and an associated fatigue crack growth law to predict the life of the components subjected to cyclic thermo-mechanical loading conditions during their service life.

2. SPECIMEN MATERIAL AND TESTING TECHNIQUES

For all tests, solution annealed AISI 316 stainless steel was used. The material composition and tensile properties are given in Table 1. The material was tested in the as received condition, soaked at 1050°C and water quenched. Specimens were machined from 16 mm plate.

The specimen was a thin plate (2 mm thick and 40 mm wide), with either 4 mm or 1 mm deep machined starter cracks, used for isothermal and thermal shock tests respectively, as shown on Fig. 1. The starter

cracks were formed by spark erosion using a 0.1 mm diameter wire as the electrode, to produce a 0.16 mm wide slot with a round end, and minimal residual stresses.

The specimen was pin loaded in a servo hydraulic test machine, which could apply cyclic or static axial tensile load up to a maximum of 60 kN. The testing machine was designed so that a variety of high temperature tests could be performed on the same facility, with independent control of both stress and temperature histories.

The specimen was heated to an initial temperature of 625°C by an induction heating coil and the temperature on the specimen was monitored by both a thermocouple and a radiation pyrometer. The pyrometer was focussed onto a 1.50 mm diameter target area on the specimen. The specimen surface was painted to a thickness of 0.05 -0.1 mm with a high emissivity oxide paint to ensure that the emissivity remained constant for the duration of the test. The emissivity was calibrated for each test by reference to the thermocouple.

For the thermal shock tests, the specimen was cooled either on one edge or on the two opposite edges by a pair of air jets from nozzles 17 mm wide x 1 mm thick. Cold compressed air at a constant 5 bar pressure was blown on the specimen edges, with the nozzles placed 0.5 mm from specimen surfaces. The cooling period of the cycle was 3 seconds followed by 57 seconds heating. Cooling was so fast that a temperature drop of 380°C at the cooled edge was achieved in 3 seconds. The growth of the fatigue crack was monitored periodically by a travelling microscope at x40 magnification, and the cyclic variation of temperature with time was recorded at 39 different positions across the specimen surface in both (x) and (y) directions.

The isothermal tests were conducted on the same test facility, but with a constant temperature and a cyclic tensile load, controlled from the load cell at one end of the specimen.

2. RESULTS

Three sets of crack growth data in the form of a vs N plots, are presented in Fig. 2(a, b, c) for single edge thermal downshock at 550, 625 and 650°C maximum temperature, showing the effects of a mean stress on growth rate and penetration of fatigue cracks. In Fig. 2(d) the crack growth results from the top edge of a double edge thermal downshock specimen at 625°C maximum temperature are shown. They may be

compared directly with the data derived from the bottom edge, Fig. 2(e), which should be identical for this symmetrical loading case. Discrepancies between top and bottom edges give an indication of inherent scatter in the test procedure. The degree of symmetry observed at both 5 and 75 MPa mean stress is very acceptable.

Two sets of data at 550 and 650°C for single edge thermal downshock have been already analysed and presented by Misumi et al [7]. For this study, the single set of SENT specimens at 625°C has been selected for a more detailed analysis, which is discussed with reference to oxide induced closure and cyclic plasticity during thermal downshock conditions.

3.1 Temperature Distribution Calculation

The temperature distribution is required for evaluation of thermal stresses, which will vary with both time and position in the specimen. One dimensional variation of temperature across the plate is considered.

The previous model [7] has been modified to fit any temperature distribution for SENT specimen in terms of (a) the maximum temperature of the thermal shock cycle, (b) the change in bulk temperature during shock, (c) the minimum temperature after completion of the cooling shock, and (d) the ambient temperature. These values are fitted to the time/space/temperature equations given by:

$$Z < 0: \quad T = T_{max}\,(1 - At) - T' \left[\frac{0.3 + 1.70\,t}{1 + 1.70\,t}\right] Z^4 \qquad (1)$$

$$Z \geq : \quad T = T_{max}\,(1 - At) \qquad (2)$$

where:

$$Z = x - 13 - x' \left[\frac{t}{1 + 2t}\right] \qquad (3)$$

$$x' = 1.26\,(T_{max} - T_a)^{1/3} \qquad (4)$$

- T – temperature in °C.
- x – Distance across specimen, measured from cooled edge, in mm.
- t – Time measured from start of cooling, in secs.
- T_{max} – Maximum temperature of the cycle, in °C, at time $t = 0$.
- A – Fitted constant to give reduction in bulk temperature during shock.

T' - Fitted constant to give observed minimum temperature at cooled edge, at end of shock period.

T_a - Ambient temperature, in ^0C.

The four constants T_{max}, A, T' and T_a were determined from separate measurements, taken in each series of tests. The remaining constants, in equations (1) to (4) were determined from analysis of temperatures recorded in four series of tests at 550, 625, 650 and 850^0C maximum temperature, for the specimen and air nozzle dimensions described above.

Fig. 3 shows the calculated temperature distribution at 625^0C for a 3 seconds cooling shock with profiles drawn for each second. Fig. 4 compared the calculated and measured temperature distribution for 650^0C, showing quite good agreement with equations 1 - 4.

In Figures 3 and 4 temperature is plotted against distance (x) across the specimen from the cooled edge. In the transverse direction (y), the profile is approximately sinusoidal in form, with a comparatively small temperature gradient, so that a one dimensional analysis for thermal stress is assumed to be acceptable.

3.2 Thermal stress calculation

An elastic approach has been undertaken to calculate the thermal stresses in the specimen arising during the thermal shock, derived from calculated temperature profiles shown in Fig. 3.

Timoshenko and Goodier's [11] equation for thermal stress has been slightly modified to suit the experimental conditions as follows:

$$\sigma_{thermal} = -E\alpha T + \frac{1}{W}\int_0^W E\alpha T \, . \, dx + \frac{12(x - 20)}{W^3}\int_0^W E\alpha T \, (x - 20) \, dx \quad (5)$$

Fig. 5 shows the thermal stress distribution for zero mean stress in the specimen, calculated from equation 5 up to 3 seconds cooling shock and plotted against the distance (x) from the cooled edge. With an end load applied, the mean stress is added directly to equation 5, by elastic superposition.

3.3 Stress Intensity Factor Calculation

By using TADA'S [12] relationship for a single edge cracked plate under a point load, the Mode I stress intensity factor was determined from the thermal stresses in the specimen, where

$$K_I = \frac{2}{\sqrt{\pi a}} \int_0^a \frac{G\left(\frac{x}{a}, \frac{a}{w}\right) \cdot \sigma_{thermal}\, dx}{\left(1 - \frac{a}{w}\right)^{3/2} \sqrt{1 - (x/a)^2}} \qquad (6)$$

where:

$$G\left(\frac{x}{a}, \frac{a}{w}\right) = g_1\left(\frac{a}{w}\right) + g_2\left(\frac{a}{w}\right)\left(\frac{x}{a}\right) + g_3\left(\frac{a}{w}\right)\left(\frac{x}{a}\right)^2 + g_4\left(\frac{a}{w}\right)\left(\frac{x}{a}\right)^3$$

$$g_1\left(\frac{a}{w}\right) = 0.46 + 3.06\left(\frac{a}{w}\right) + 0.84\left(1 - \frac{a}{w}\right)^5 + 0.66\left(\frac{a}{w}\right)^2\left(1 - \frac{a}{w}\right)^2$$

$$g_2\left(\frac{a}{w}\right) = -3.52\left(\frac{a}{w}\right)^2$$

$$g_3\left(\frac{a}{w}\right) = 6.17 - 28.22\left(\frac{a}{w}\right) + 34.54\left(\frac{a}{w}\right)^2 - 14.39\left(\frac{a}{w}\right)^3 - \left(1 - \frac{a}{w}\right)^{3/2} - 5.88\left(1 - \frac{a}{w}\right)^5 - 2.64\left(\frac{a}{w}\right)^2\left(1 - \frac{a}{w}\right)^2$$

$$g_4\left(\frac{a}{w}\right) = -6.63 + 25.16\left(\frac{a}{w}\right) - 31.04\left(\frac{a}{w}\right)^2 + 14.41\left(\frac{a}{w}\right)^3 + 2\left(1 - \frac{a}{w}\right)^{3/2} + 5.04\left(1 - \frac{a}{w}\right)^5 + 1.98\left(\frac{a}{w}\right)^2\left(1 - \frac{a}{w}\right)^2$$

where

K_I - Mode I stress intensity factor

a - crack length, mm

w - width of the specimen, mm.

Fig. 6 shows the stress intensity factor profiles for the minimum and maximum thermal stresses, at the start and finish of the thermal shock respectively, for the case of zero end load. This may be compared with Figs. 7 and 8, showing the K-profiles with 5 and 120 MPa mean stress due to static end loads. The stress intensity factor is plotted as a function of the crack length a, measured from the cooled edge.

3.4 Isothermal Results

Fig. 9 shows the plots of crack growth rate (da/dN) against the range of stress intensity factor (ΔK), for isothermal tests at 350, 450, 550 and 650°C. The crack growth rate in the isothermal tests was calculated with a 5-point polynomial fit, using the method described in ASTM E647 [13]. Stress intensity factor calculations were made by using the Brown and Srawley solution [12] for the single edge cracked plate under tension, as given by:

$$K_1 = \sigma \sqrt{\pi a} \cdot F(a/w) \qquad (7)$$

$$F(a/w) = 1.22 - 0.231\,(a/w) + 10.55\,(a/w)^2 - 21.71\,(a/w)^3 + 30.382\,(a/w)^4.$$

where:

$\Delta K = K_{max} - K_{min}$

σ = Applied tensile stress, MPa

Testing conditions for the isothermal tests are described in Table 2, for load controlled sinusoidal cycling at 0.3 Hz with an R-ratio of 0.1.

Fig. 10 presents the crack growth rate plotted against the range of strain intensity factor, which is defined by the simple relationship.

Strain intensity factor range = $\Delta K/E$ (8)

where (E) is the Young's modulus at the respective temperature for each test. By the use of a strain intensity, the dependence of crack growth on temperature is reduced to some extent.

4. DISCUSSION

The results for four sets of crack growth data have been presented for single edge thermal shock at 550, 625 and 650°C and for double edge cooling at 625°C. The effect of static mean stress in both types of test can be seen in Figs. 2. By increasing the mean stress, the speed and penetration of the cracks is raised. It also shows that the crack growth rate is higher where the temperature gradient is much more severe, close to the cooled edge, and as the crack grows towards the low thermal gradient and compressive stress region (Fig. 5) it slows down and arrests.

The crack growth rate during thermal shock can be interpreted by the stress intensity factor variation with increasing crack length. Figs. 6, 7 and 8 show the K_{max} and K_{min} profiles for zero, 5 and 120 MPa mean stresses, from which the range of stress intensity factor can be derived. This predicts a maximum crack growth rate for a = 2.5 mm, followed by deceleration as ΔK gradually decreases. This agrees with the crack growth results in Fig. 2(b), where the crack advances rapidly up to 3 mm, then decreases towards the threshold value and stops.

The effect of mean end load on fatigue crack propagation can also be deduced from Figs. 7 and 8. Both figures show the same sharp increase in the crack length and subsequent deceleration, as ΔK is identical in each case. But for higher end load, the R-ratio is

greatly increased, so that instead of showing the tendency to arrest, cracks may move towards final fracture. Final fracture may only occur if the threshold stress intensity factor range, which is a function of R-ratio, is sufficiently reduced to ensure that ΔK does not fall below this threshold. The same behaviour has been reported by Marsh [5].

Isothermal tests were conducted in the temperature range of 350 -650°C, with the stress range taken as 2/3 of the yield at the respective test temperature. It has been reported [14] that austenitic stainless steel shows an ageing effect in early stages of high temperature tests. In Figs. 9 and 10 the isothermal results are shown which illustrate that in the very early stages of the test (i.e. first 48 hours), we have a discrepancy in the value of growth rate. In that region the speed of the crack is higher at the respective temperatures, whereas in the later stages of life the crack speed is almost the same for all temperatures, when plotted on a strain intensity basis. The longer test times with retarded growth rates are applicable to the thermal shock tests, where at a frequency of 1 cycle per minute ageing processes were very quickly completed.

During thermal shock conditions, the material experiences stresses well beyond yield. It is believed that we get a significant amount of cyclic plasticity around the crack tip during propagation. Under such conditions, if the prediction of crack growth is made on the basis of a stress intensity approach, it will show that the calculated life of the components subjected to thermal shock is over estimated. Therefore, to take account of cyclic plasticity around the crack tip, a strain intensity based approach is proposed [15, 16].

In Fig. 11, isothermal and thermal shock test results are correlated on the basis of a strain intensity factor approach. This shows that the thermal shock test with 120 MPa end load is in agreement with the long term isothermal test results at 350, 450 and 550°C, which is the range of mean temperature during the thermal downshock cycle. However, the isothermal test at 650°C is forming an upper bound, which is nearly equal to the maximum temperature of the cycle.

The thermal shock test with 5 MPa end load shows some agreement in the early fast crack growth region, but subsequently the crack growth rate falls steadily away to give a final difference in magnitude of the order of 2 compared to isothermal results. The most feasible reason for this type of behaviour is because the duration of low mean stress

thermal shock tests is about 10 to 12 weeks, so that the material oxidises on the fracture surfaces with the passage of time and forms a thick oxide layer on the surface behind the crack tips. Thus when the crack reaches the low thermal gradient and compressive stress region, the propagation rate slows down as the effective ΔK is reduced due to oxide induced closure, until the crack stops propagating. But when the higher mean end load is introduced in the low thermal gradient region, the crack propagates to a greater length before the threshold is achieved since closure is not able to occur. A calculation of the crack tip opening displacement for the final crack length of 7 mm in Fig. 2(b) under the low mean stress indicates that oxide layers of only 2 μm thickness are needed to provide the crack growth rate reduction observed in Fig. 11.

5. CONCLUSIONS

1. A steep temperature gradient gives higher crack growth rates in thermal shock.
2. Superimposed static mean stress increases the speed and penetration of the crack.
3. Oxide induced crack closure is significant at low mean stresses under thermal shock conditions for 316 stainless steel.
4. Thermal shock can be analysed by strain intensity approach with isothermal data for crack propagation.

ACKNOWLEDGEMENTS

Financial support from the Ministry of Science and Technology of Pakistan for one of the authors (S. T. HASAN) is greatly acknowledged.

REFERENCES

[1] Emery, A. F., Walker, G. E. and Williams, J. A. (1969). J. Basic Engg., Trans. ASME, Series D.91, 618 - 624.

[2] Howes, M. A. H., (1973). Fatigue at Elevated Temperatures, ASTM-STP 520, 242 - 254.

[3] Mowbray, D. F., Woodford, D. A. and Brandt, D. E. (1973). Fatigue at Elevated Temperature, ASTM-STP 520, 416 - 426.

[4] Skelton, R. P. (1983). Fatigue at High Temperature, Ed. R. P. Skelton, Applied Science Publishers, 1 - 62.

[5] Marsh, D. J., (1981). Fatigue of Engg. Materials and Structure, vol. 4, No. 2, 179 - 195.

[6] Bizon, P. T. and Spera, D. A., (1976), Thermal Fatigue of Materials and Components, ASTM STP 612, 106 - 122.

[7] Misumi, M., Nakamura, Y., Brown, M. W. and Miller, K. J. (1986). Symposium of Fracture and Fatigue Mechanics, June 30 - July 2, Tokyo, 261 - 266 (in Japanese).

[8] Shimizu, M., Brown, M. W. and Miller, K. J. (1983). Mechanical Behaviour of Materials - IV, vol. 1, Stockholm, Sweden, 15 - 19 Aug. 1983, 207 - 213.

[9] Skelton, R. P. (1979). Proc. ICM 3, Cambridge, Pergamon, vol. 2, 13 - 22.

[10] Marsh, D. J. and Charlesworth, F. D. W., (1985), Multiaxial Fatigue, ASTM STP 853, 700 - 719.

[11] Timoshenko, S. P. and Goodier, J. N., Theory of Elasticity, 3rd edition, McGraw-Hill.

[12] Tada, H., Paris, P. and Irwin, G., The Stress Analysis of Cracks Handbook, 1985, Del. Research Corporation.

[13] E647-83, 1983 Annual Book of ASTM standards, part 10, 765 - 783.

[14] Rios, E. R. de los and Brown, M. W., (1981), Fatigue of Engg. Materials and Structure, vol. 4, No. 4, 377 - 381.

[15] Skelton, R. P., (1982), Low Cycle Fatigue and Life Prediction, ASTM STP 770, 337 - 381.

[16] Hobson, P. D., Brown, M. W. and Rios, E. R. de los, (1981). The Behaviour of Short Fatigue Cracks, EGF Publication 1, Editors, K. J. Miller and E. R. de los Rios, Mechanical Engineering Publications, 441 - 459.

Table 1

Chemical Composition and Mechanical Properties

C	Mn	Ni	Cr	Mo	Si	S	P
0.049	1.36	11.20	17.26	2.15	0.54	0.018	0.023

Temperature °C	0.2% Proof Stress MPa	Tensile Strength MPa	Elongation %	Red in area %
20	243	597	68	71
371	142	513	37.7	67
427	137	504	39.9	65
550	133	474	44	55
649	117	316	27	48.7

Table 2

Isothermal Testing Conditions

Test No.	Temperature °C	Max. Tensile Stress MPa	Min. Tensile Stress MPa	Stress Range MPa
M-7	350	83.33	8.33	75.0
M-8	450	83.56	8.36	75.2
M-9	550	76.33	7.63	68.7
M-10	650	68.16	6.81	61.35

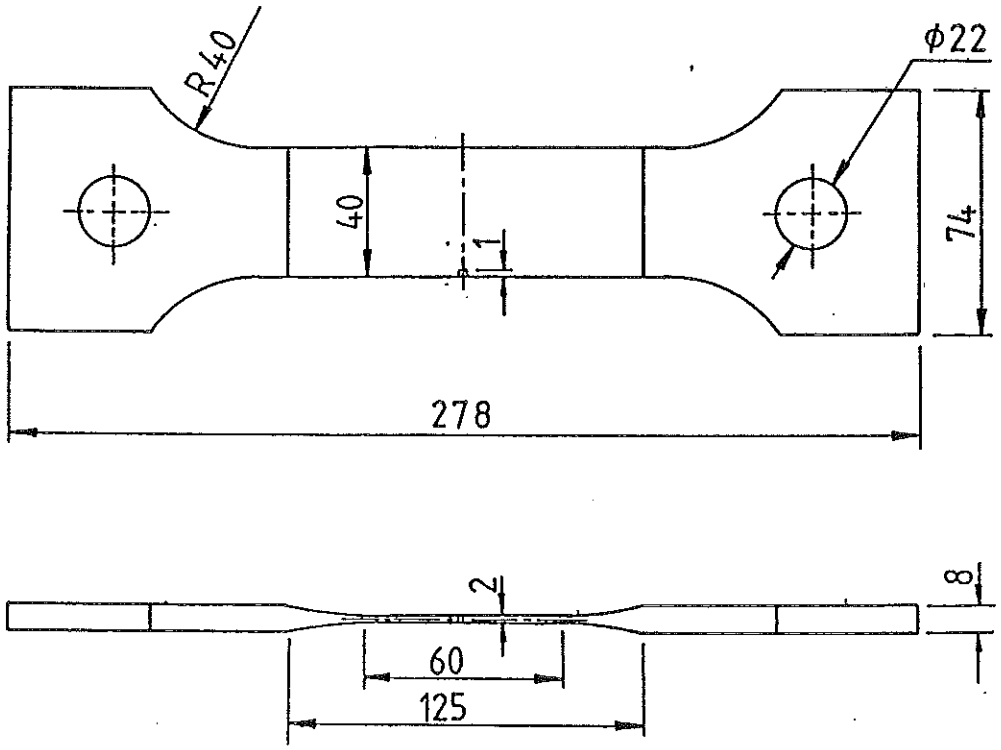

FIG. 1 SPECIMEN DIMENSIONS (IN MILLIMETRES)

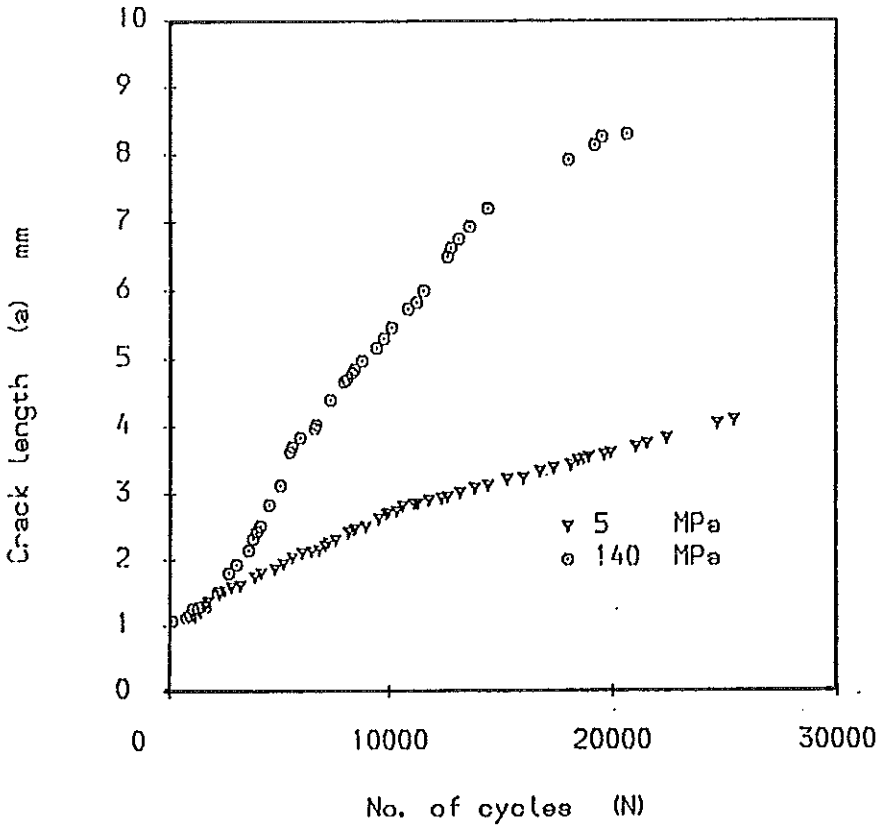

Fig - 2 (a) SINGLE EDGE THERMAL SHOCK RESULTS AT 550 °C (MAX)

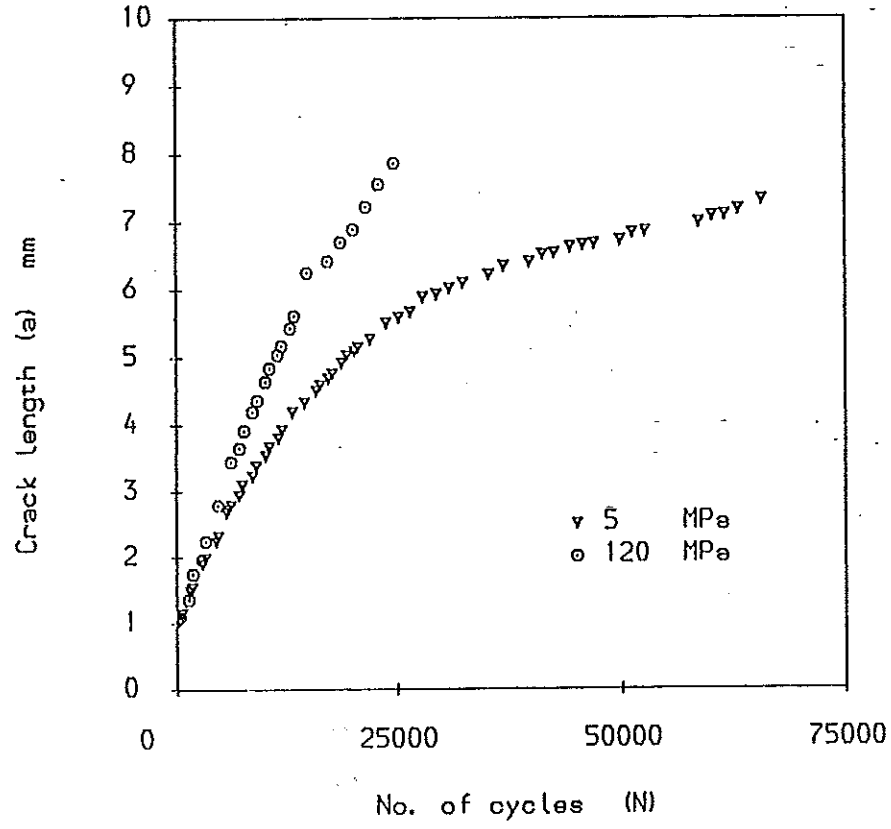

Fig - 2 (b) SINGLE EDGE THERMAL SHOCK RESULTS AT 625 °C (MAX)

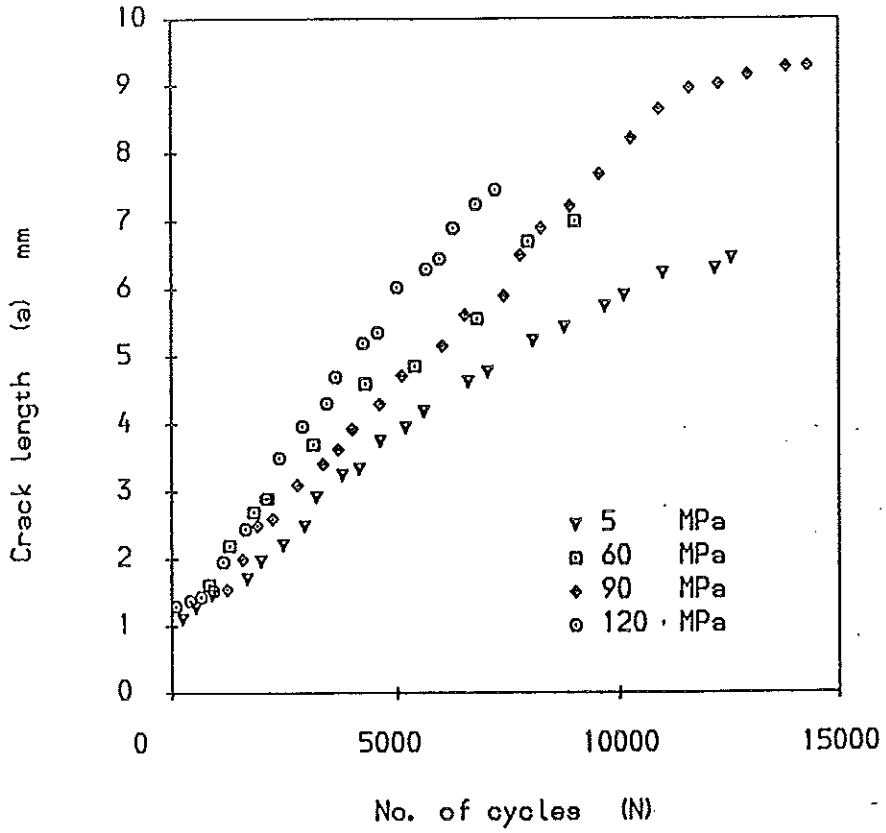

Fig - 2 (c) SINGLE EDGE THERMAL SHOCK RESULTS AT 650 °C (MAX)

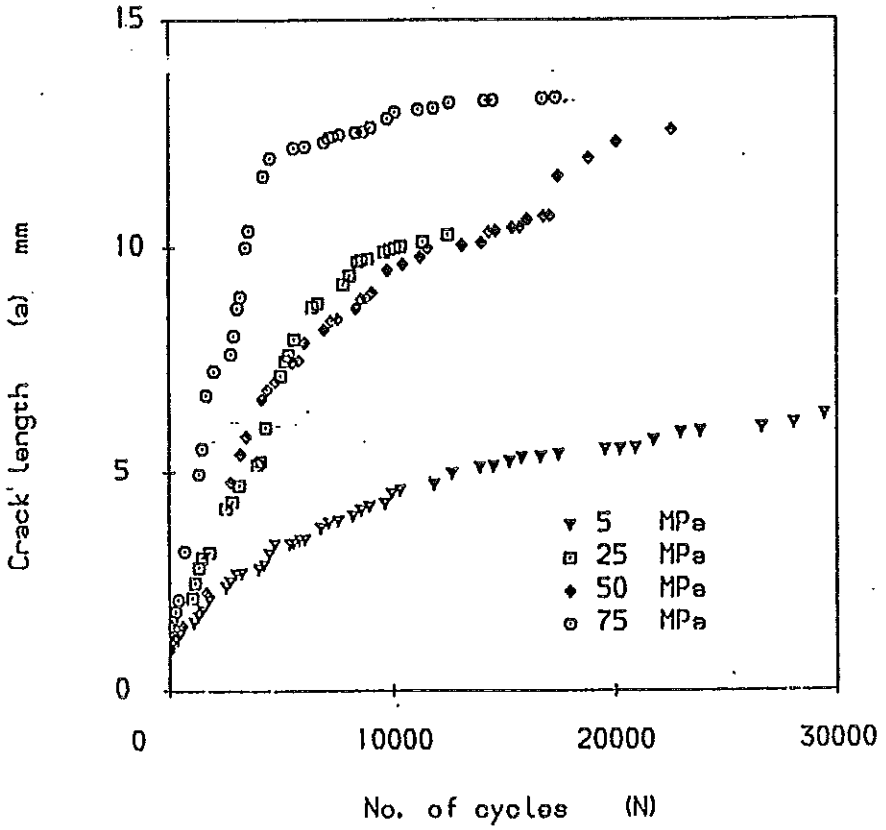

Fig - 2 (d) DOUBLE EDGE THERMAL SHOCK RESULTS

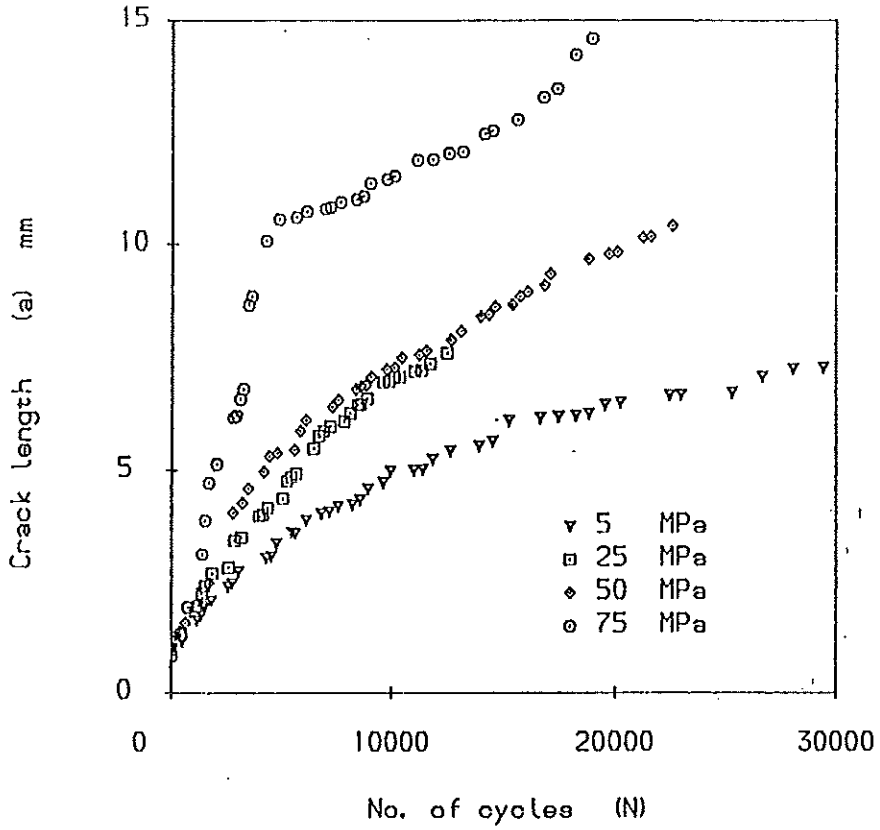

Fig - 2 (a) DOUBLE EDGE THERMAL SHOCK RESULTS (B.E)

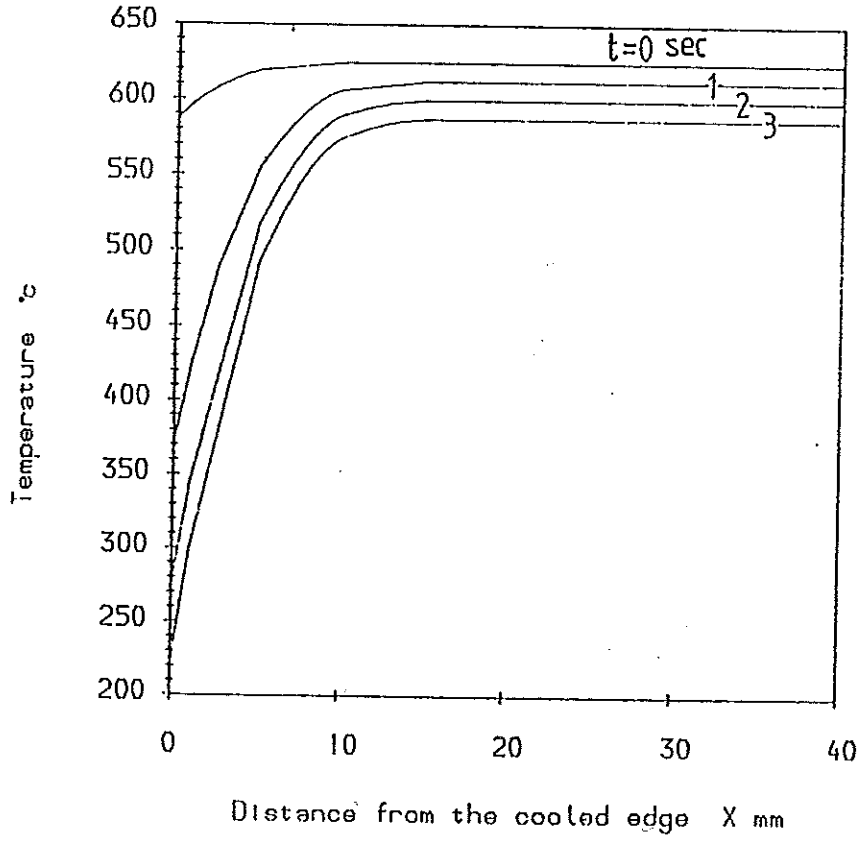

Fig - 3 TEMPERATURE DISTRIBUTION AT 625 °C (MAX.)

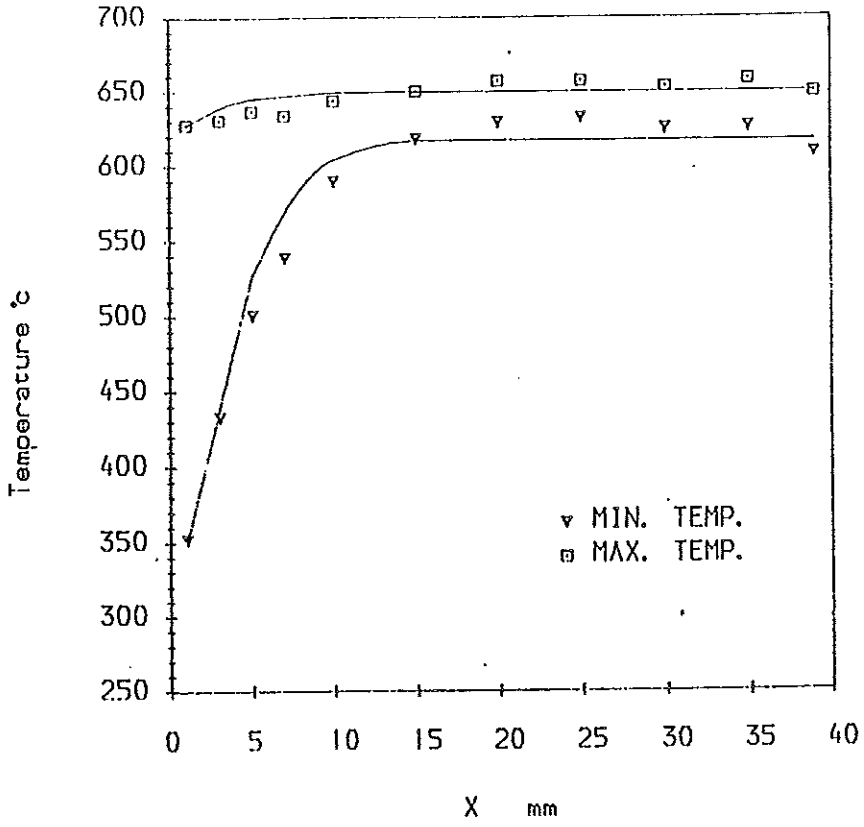

Fig. - 4 TEMPERATURE DISTRIBUTION AT 650 °C

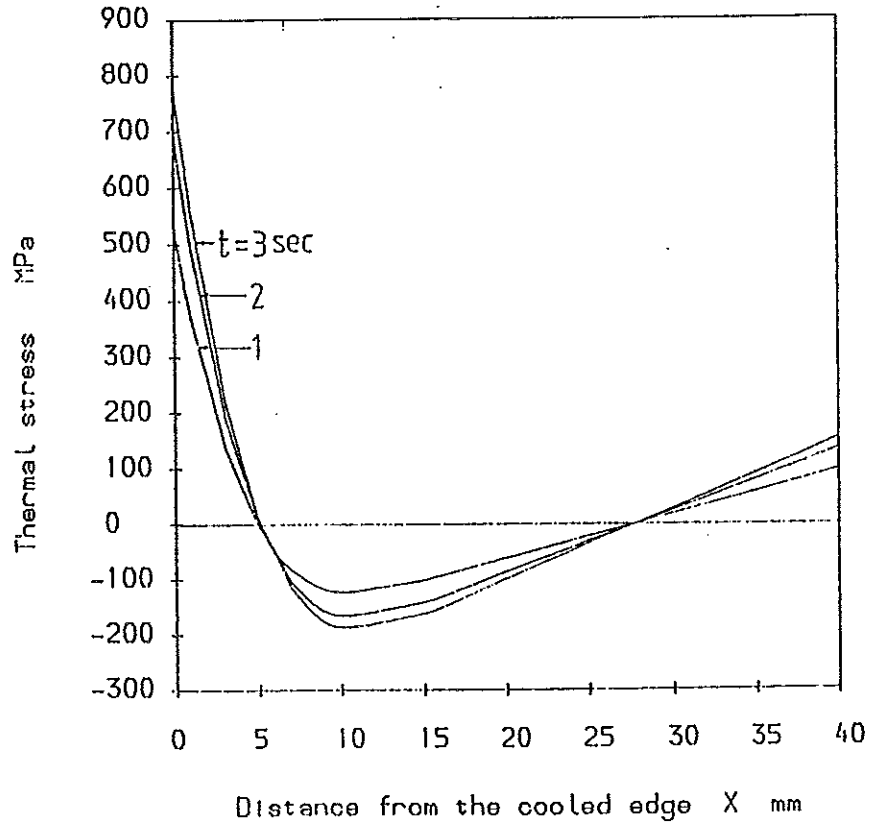

Fig - 5 THERMAL STRESS PROFILE FOR 0 MEAN STRESS

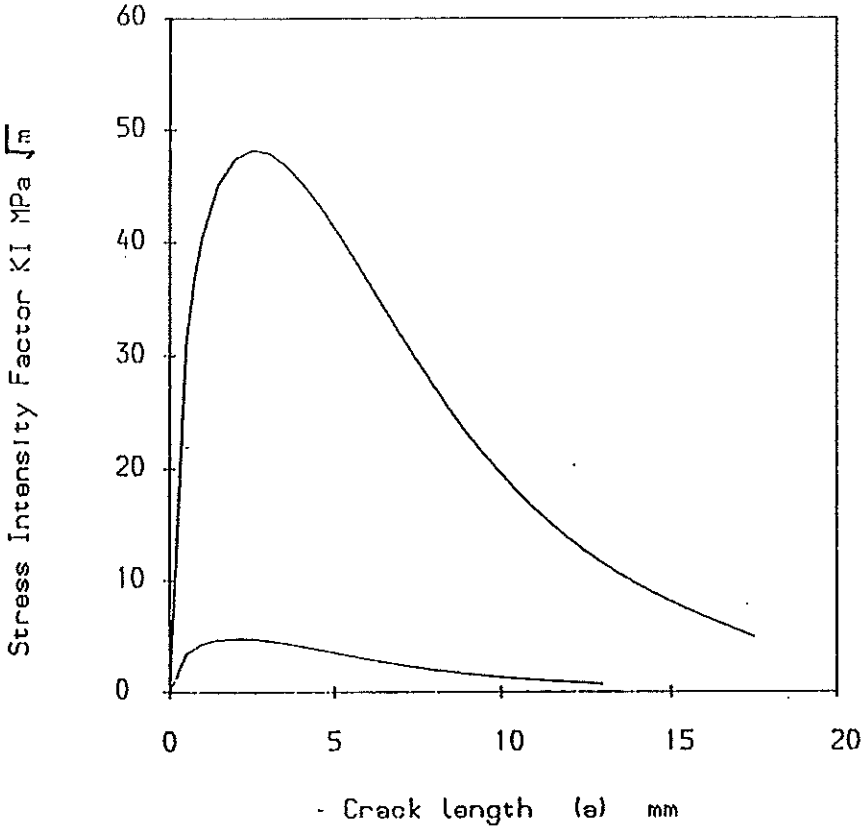

Fig - 6 STRESS INTENSITY FACTOR PROFILES FOR 0 MEAN STRESS

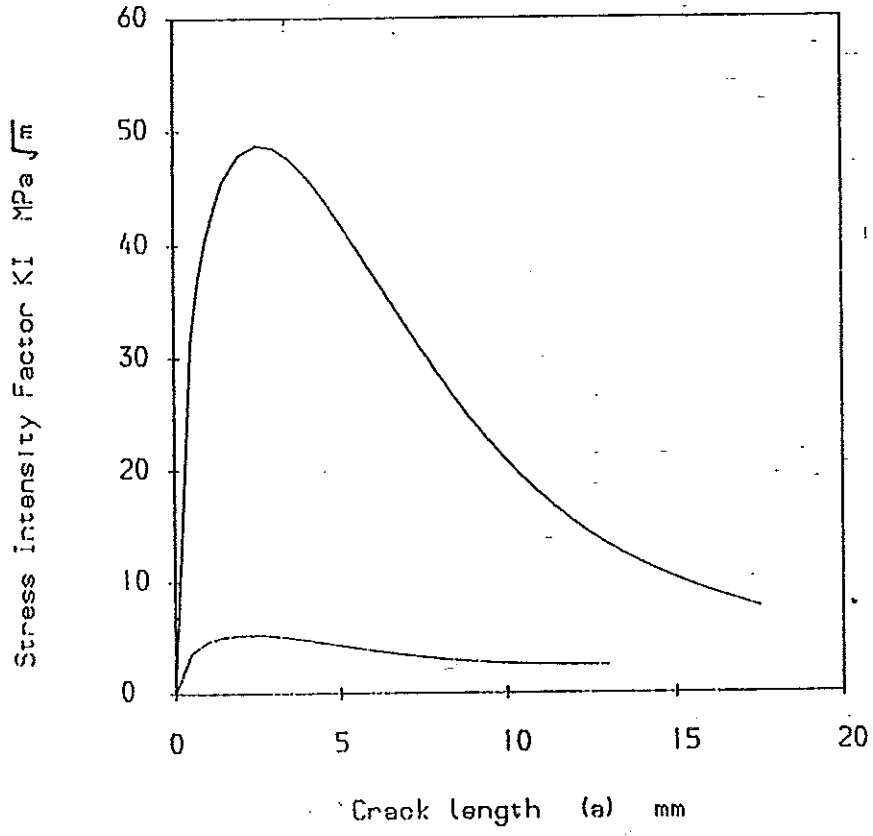

Fig - 7 STRESS INTENSITY FACTOR PROFILES FOR 5 MPa MEAN STRESS

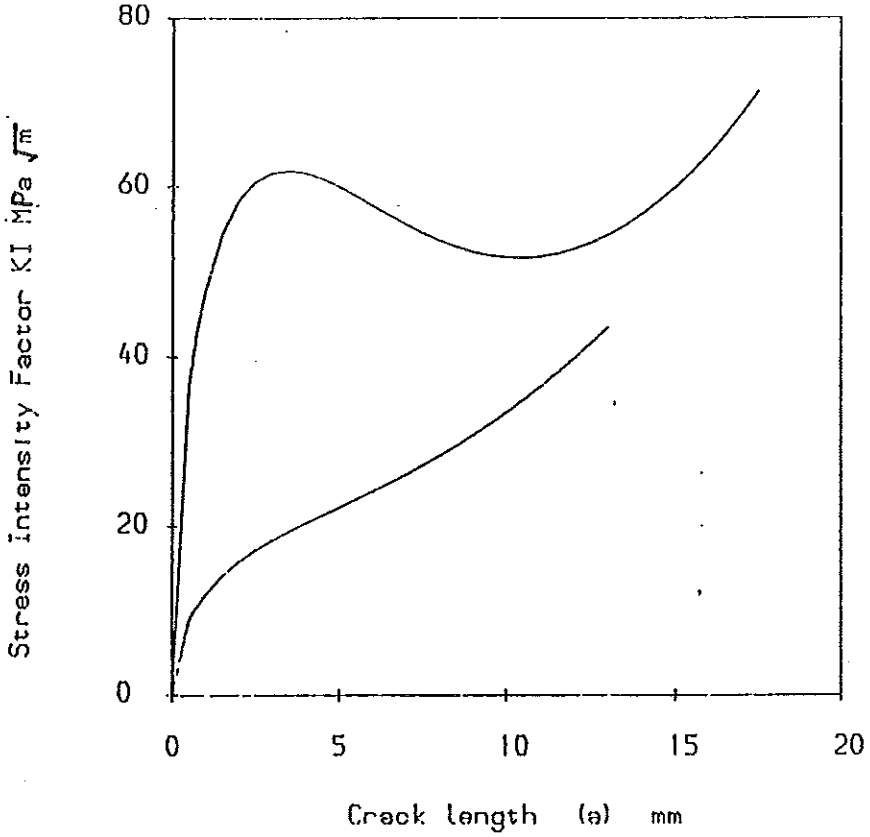

Fig - 8 STRESS INTENSITY FACTOR PROFILES FOR 120 MPa MEAN STRESS

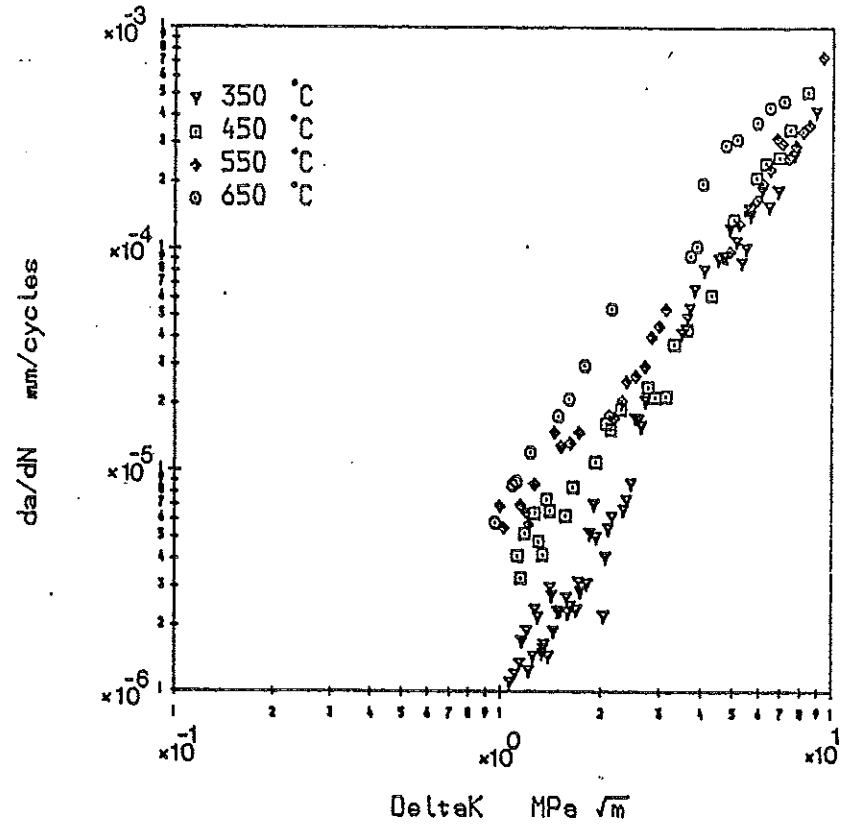

Fig - 9 ISOTHERMAL DATA

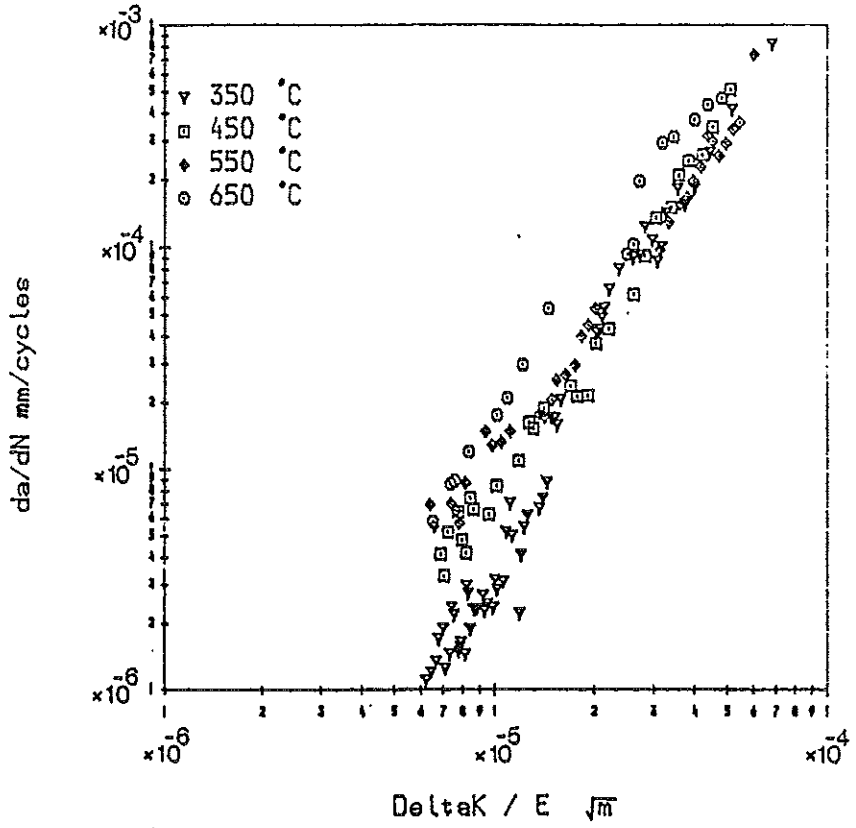

Fig - 10 ISOTHERMAL DATA

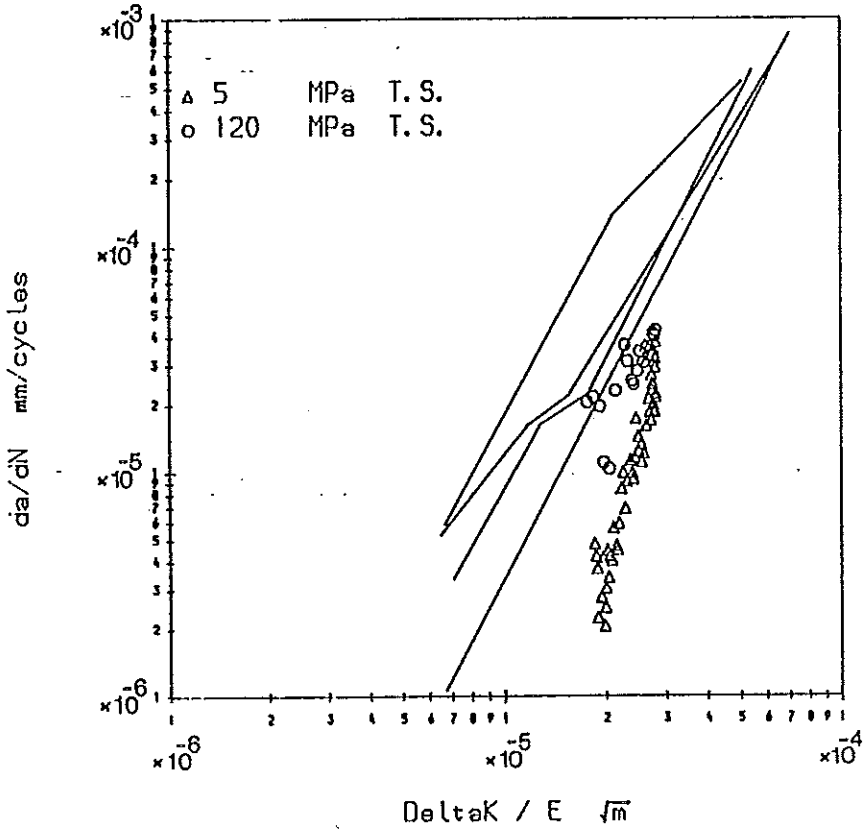

Fig - 11 CORRELATION OF THERMAL SHOCK RESULTS WITH ISOTHERMAL DATA